Journal of Power Sources 222 (2013) 150–160

Contents lists available at SciVerse ScienceDirect

Journal of Power Sources

journal homepage: www.elsevier.com/locate/jpowsour

Numerical investigation of water dynamics in a novel proton exchange membrane fuel cell flow channel

Yanzhou Qin [a,b], Qing Du [a], Yan Yin [a], Kui Jiao [a], Xianguo Li [a,b,*]

[a] State Key Laboratory of Engines, Tianjin University, 92 Weijin Road, Tianjin 300072, China
[b] Department of Mechanical and Mechatronics Engineering, University of Waterloo, Waterloo, ON, Canada

HIGHLIGHTS

- Water transport and dynamics in a novel PEMFC flow channel is simulated numerically.
- The novel flow channel consists of a hydrophilic needle in the flow channel.
- Water emerging from MEA surface is removed by the hydrophilic needle upon contact.
- Optimal needle diameter and length are determined.

ARTICLE INFO

Article history:
Received 22 April 2012
Received in revised form
29 July 2012
Accepted 30 July 2012
Available online 7 August 2012

Keywords:
Proton exchange membrane fuel cell
Water management
Water removal
Water dynamics
Numerical simulation
Channel flow

ABSTRACT

Water dynamics in the flow channel of a proton exchange membrane fuel cell is significantly important to water management and removal. In this study, volume-of-fluid method is used to investigate numerically the three-dimensional water dynamics in a flow channel with a hydrophilic needle. It is found that water transport and dynamics in this novel flow channel are quite different from the conventional channel. Liquid water droplet, introduced on the electrode surface, is removed through capillary effect once touching the hydrophilic needle. This is desirable since the electrode surface becomes free of liquid water, avoiding the flooding and blockage of reactant gas transport into the electrode. Increasing the contact area between the water droplet and needle, through an increase in the diameter or length of the needle, can facilitate water removal from the electrode surface because of greater capillary effect, but it also increases the pressure drop in the channel due to greater blockage by the needle. Overall, the pressure drop in the modified channel is still small compared to the pressure drop in a serpentine flow channel, making the present approach viable for use in the conventional parallel flow channels for proton exchange membrane fuel cells.

© 2012 Elsevier B.V. All rights reserved.

1. Introduction

Proton exchange membrane fuel cell (PEMFC) is one of the promising candidates as zero-emission power source for transportation, stationary co-generation and portable applications due to its high efficiency, low-operating temperature and rapid start-up features. However, further research and development effort is needed to make it more practical, durable, and economical for broader commercialization [1,2].

Water management is one of the critical issues for fuel cell design and optimization, and has been extensively studied both experimentally and numerically in the past decades. In a PEMFC, the membrane must be well hydrated to ensure high protonic conductivity. On the other hand, due to the low operating temperature and production of product water, excessive humidification can result in water flooding of cathode structure that can subsequently block the cathode gas flow channel; this phenomenon results in a lower air flow rate in the blocked channel for the parallel flow channel configuration, leading to more water accumulation in the blocked channel, thus decreasing the cell performance; and a higher pressure drop in the blocked channel for the serpentine flow channel configuration, then higher parasitic energy consumption for the cathode flow, decreasing the overall system performance. Therefore, proper water management must be implemented to improve the PEMFC performance.

Water transport occurs in proton exchange membrane, in gas diffusion layer (GDL) and in gas flow channel of a PEMFC. Water

* Corresponding author. State Key Laboratory of Engines, Tianjin University, 92 Weijin Road, Tianjin 300072, China. Tel.: +86 22 8740 2029; fax: +86 22 2740 6949.
E-mail address: x6li@tju.edu.cn (X. Li).

0378-7753/$ – see front matter © 2012 Elsevier B.V. All rights reserved.
http://dx.doi.org/10.1016/j.jpowsour.2012.07.084

management is one of the critical issues for the design and optimization of PEMFCs, and has been investigated by both experiments and numerical simulations. By far, extensive studies have been carried out on the water transport in the membrane [3–5] and GDL [6–17]. As for water transport in the gas flow channel, only vapor phase water was considered in earlier studies, such as those by Bernardi and Verbrugge [18,19] and Springer et al. [3]. More recently, the study of water management in the gas flow channel has been extended to two-phase flow. Zhang et al. [20] constructed a transparent cell and by virtue of high-speed charged coupled device (CCD) camera, they observed the liquid water transport inside the gas flow channel and on the surface of the GDL as well. Hussaini and Wang [21] also used direct in situ visualization technology to investigate the cathode gas flow channel flooding of a PEMFC, they classified water flow in the channel into four flow patterns according to the channel images and they achieved a qualitative description of flow patterns called a flow map in terms of PEMFC operating conditions. Water droplet flow on the membrane-electrode assembly (MEA) surface was identified in the channel images in [20,21]. Jiao et al. [22] used a transparent plate as the bipolar plate for PEMFC to reveal the liquid water flow on the MEA surface, especially the liquid water flow under the land by the cross flow, indicating that the cross flow had significant effects on water removal. The work of Zhang et al. [23] also discovered water flooding in PEMFC. Quan et al. [24] simulated the water behavior in a U-shaped air flow channel by using volume of fluid (VOF) method for the first time. This work provided useful insights for understanding two-phase water behavior and introduced a new method for water management study in a PEM fuel cell. Jiao et al. [25,26] simulated the two-phase water transport in the manifolds and flow stacks. By using the same approach, the channel wall wettability, the MEA surface wettability, and the gas inlet velocity on the water behavior and removal in the flow channel were investigated by Zhan et al. [27], Cai et al. [28] and Mondal et al. [29]. Many designs of the geometry of the gas flow channel were carried out to improve the water management and gas distribution in PEMFC recently [30–35].

Gas flow channel is known to have important influence on water management and removal in PEMFC and better designs of the flow channel could enhance the cell performance. Consequently, various designs and layouts of the flow channel have been developed [36]. In this study, a conventional gas flow channel is modified by inserting a hydrophilic needle (small cylinder) in the middle of the channel to improve water management and removal in the channel; since liquid water droplet emerging from the hydrophobic MEA surface, once in contact with the hydrophilic needle surface, will be dragged away and removed from the MEA surface. Water transport and dynamics, especially water removal process from the MEA surface, in the modified channel are numerically investigated by using the VOF method. The effect of the diameter and the length of the needle is studied as well and the dimensions of the needle are optimized.

2. Model formulation

2.1. Physical problem

Fig. 1 shows a schematic of the transport phenomena in the cathode side of a PEMFC. The reactant oxygen from the air (usually humidified) is transported from the gas flow channel, passing through the GDL, to the catalyst layer (CL), where it is consumed by the electro-chemical reaction. The product water from the electro-chemical reaction and water from the membrane by the electro-osmotic drag (EOD) effect are transported to the gas flow channel, in both vapor phase by diffusion and liquid phase by permeation. Due to the relative low temperature in PEMFC, the water vapor could further be condensed in the GDL and on the MEA surface. Water droplet and water film flow on the MEA surface could be formed. If the water on the MEA surface could not be effectively removed, it would block the reactant gas transport into the MEA, and thus decrease PEMFC performance significantly. In this study, a novel method to accelerate the water removal process from the MEA surface is implemented by inserting a hydrophilic needle in the middle of the gas flow channel.

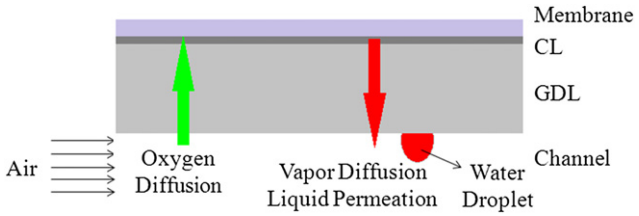

Fig. 1. Schematic of water transport in the cathode side of a PEM fuel cell. CL stands for catalyst layer and GDL stands for gas diffusion layer.

2.2. Computational domain and assumptions

Fig. 2 illustrates a schematic of the 3D computational domain showing a typical straight cathode channel of rectangular cross section in a PEMFC. The channel is 50 mm long with 1 mm × 1 mm square cross section. For the base case considered in this study, a small cylindrical needle with the diameter of 0.1 mm and the length of 0.7 mm, normal to the channel bottom wall, is inserted in the middle of the flow channel, 4 mm away from the air inlet. In general, water droplet emerges in the flow channel from the reaction zone through the GDL. At time $t = 0$, a droplet is introduced on the MEA surface, near the inlet of the flow channel for all simulations. For the sake of simplicity, only one droplet is considered in this study and the vaporization is not considered since the air in the channel is regarded fully humidified. The motion of gas and water is considered to be an incompressible Newtonian flow and these two phases are separated by an interface having a constant surface tension coefficient. The air flow in the channel is considered as laminar ideal gas under isothermal condition and there is no phase change between the two phases considering the high relative humidity for the fully humidified gas streams in PEM fuel cell operations. Therefore, the conservation of mass and momentum are the governing equations for the channel flow.

2.3. Governing equations

The conservation equations governing the channel flow can be written as:

$$\text{Continuity equation}: \quad \frac{\partial \rho}{\partial t} + \nabla \cdot (\rho \vec{v}) = 0 \tag{1}$$

$$\text{Momentum equation}: \quad \frac{\partial (\rho \vec{v})}{\partial t} + \nabla \cdot (\rho \vec{v} \cdot \vec{v}) = -\nabla P + \mu \nabla \cdot \left(\nabla \vec{v} + \nabla \vec{v}^{\mathrm{T}} \right) + \rho \vec{g} + \vec{F}_s \tag{2}$$

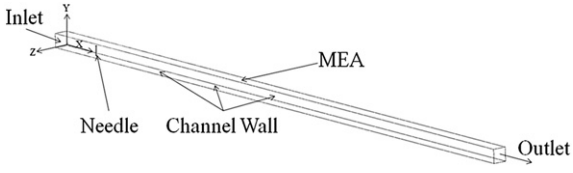

Fig. 2. Computational domain considered in the present study.

where ρ (kg m^{-3}) is the density, $\vec{v}$(m s^{-1}) is the velocity vector, P(Pa) is the static pressure, μ (kg m^{-1} s^{-1}) is the viscosity, $\vec{g}$(m s^{-2}) is the gravity, and $\vec{F}_s$(N m^{-3}) is a source term representing the surface tension effect and only acting on the interface between the two phases. The above two equations govern the motion of both air and liquid water in the flow channel. The liquid droplet may deform while moving in the channel and its instantaneous surface is determined by the volume of fluid (VOF) method as described below.

2.4. Volume-of-fluid method

To track the air–water two-phase flow interface inside the computational domain, the VOF method is used in the present study. The VOF method is designed for two or more immiscible fluids, and the tracking of the interface is accomplished by the solution of a continuity equation for the volume fraction of one (or more) of the phases.

The volume fraction continuity equation is given as:

$$\frac{\partial f_1}{\partial t} + \nabla\cdot(f_1\vec{v}) = 0 \tag{3}$$

where f_1 is the volume fraction of the fluid 1, which is taken as liquid water in the present study. The volume fraction is introduced to capture the interface movement. Here, $f_1 = 0$ indicates that the control volume is filled with only air, $f_1 = 1$ indicates that the control volume is full with liquid water, and f_1 between zero and unity indicates that the control volume contains the interface between the two fluids. The sum of the volume fractions is equal to 1, since there are only two phases, the volume fraction of the air, f_2, can be obtained based on the following relationship:

$$f_1 + f_2 = 1 \tag{4}$$

The volume fraction equation is solved through explicit time discretization. All the other properties (e.g., viscosity) can be computed in a volume fraction weighted-average manner, if the volume fraction of the fluid 2 is being tracked, for example:

$$\mu = \mu_1(1 - f_2) + \mu_2 f_2 \tag{5}$$

The surface tension effect is considered as a source term in the momentum equation. For two-phase flow, it can be expressed as [37]:

$$\vec{F}_s = \sigma\frac{\rho\kappa\nabla f_2}{0.5(\rho_1 + \rho_2)} \tag{6}$$

where σ (N m^{-1}) is the surface tension coefficient and κ is the surface curvature at the interface between the two phases. κ can be expressed as [37]:

$$\kappa = \nabla\cdot\vec{n} = \nabla\left(\vec{n}_w\cos(\theta) + \vec{t}_w\sin(\theta)\right) \tag{7}$$

where $\vec{n}$ is the unit vector normal to the interface between the two phases near the wall, $\vec{n}_w$ is the unit vector normal to the wall, $\vec{t}_w$ is the unit vector tangential to the wall, and θ is the static contact angle at the walls. The static contact angle could affect the surface tension, and thus influence on water transport and dynamics in the flow channel [14].

2.5. Boundary and initial conditions

The current governing equations are elliptic partial differential equations, and hence, boundary conditions are required for all of the boundaries of the computational domain. The MEA surface is also considered as a non-penetrating wall to simplify the calculation. The boundary conditions for all the regions of the computational domain are as follows:

$$\text{At the inlet}: \quad v_x = v_{x,0} = \text{const.}, \quad v_y = v_z = 0. \tag{8}$$

$$\text{At the outlet}: \quad \frac{\partial v_x}{\partial x} = 0,\ v_y = v_z = 0,\ P_{\text{out}} = \text{const.} \tag{9}$$

$$\text{At the walls}: \quad v_x = v_y = v_z = 0. \tag{10}$$

Initially ($t = 0$), the velocity and gauge pressure in the channel are set as zero and a spherical liquid water droplet with the diameter of D_{droplet} is introduced in the middle of the MEA surface, 1 mm away from the gas inlet. At $t > 0$, the air flow at the inlet is considered to be uniform with a given velocity of $v_{x,0}$. The wettability of the channel surface, the needle surface and the MEA surface can all be adjusted by setting different contact angles at their surface. The gravity force is considered along the negative y-direction. The absolute pressure at the channel exit is maintained at a pre-selected value of P_{out}.

3. Numerical

In this study, the numerical solution is carried out in FLUENT environment. The VOF method is used to simulate the water droplet transport in the flow channel. The numerical techniques used and grid independence study are reported in the following subsections.

3.1. Numerical technique

The unsteady governing equations are solved using a pressure-based solver and the explicit scheme-based VOF method is selected for the multiphase simulation. Air is considered as the primary phase and liquid water as the secondary phase. In all the simulations, the wall adhesion is considered and the surface tension coefficient between the air and water is taken as a constant value. The pressure implicit with split operator (PISO) scheme is used to obtain the pressure–velocity coupling. The pressure discretization is obtained by using the pressure staggering option (PRESTO) scheme. The second-order upwind scheme is used to solve the momentum equation and the volume fraction at the interface is calculated using the geometric reconstruction (Geo-Reconstruct) scheme. This scheme could construct the interface between fluids using a most accurate piecewise-linear approach. The interface between the two phases is assumed to be a linear slope within each cell. Based on the information of the volume fraction and its derivatives in each cell, the position of the linear interface relative to the center of the partially-filled cell is calculated. Then for the next time step, the amount of fluid advected through each face is calculated by using the computed linear interface representation and the information about the normal and tangential velocity distribution on the face and the volume fraction in each cell is calculated using the balance of fluxes obtained during the previous time step. The time step used is 10^{-5} s in this study.

3.2. Grid independency test

About 1.4 million structured hexahedral cells are meshed in the computational domain. The meshes are refined near all the wall surface area and around the needle in order to reduce the numerical error and improve the accuracy of the solutions. Grid independency is tested by increasing and decreasing the number of grid cells by 20% in every direction for all the cases considered in this

study. The flow phenomena of liquid water and the velocity field are almost the same and the difference in the pressure drop in the channel is very small (within ±1%) for each case.

There is a grid criterion for laminar boundary layer to ensure that the boundary layer is resolved during the numerical computation [37],

$$y_P\sqrt{\frac{u_\infty}{\nu x}} \le 1 \tag{11}$$

where y_P is the distance to the wall from the adjacent cell centroid, u_∞ is the free-stream velocity, ν ($m^2\ s^{-1}$) is the kinematic viscosity of the fluid (air) and x is the distance along the wall from the starting point of the boundary layer. Since the boundary layer starts at the channel inlet, and grows in the flow direction, the first computational cell near the channel inlet and adjacent to the channel wall is most difficult to satisfy because of the small value of x in Eq. (11). Once this first cell satisfies the criterion, Eq. (11), then all the downstream cells will automatically satisfy this criterion as well. The computational grid discussed early, as shown in Fig.3, satisfies the criterion given in Eq. (11). It might be mentioned that for the first cell near the flow inlet, the free-stream velocity u_∞. Eq. (11) can be approximated as the velocity at the inlet, $v_{x,0}$.

4. Results and discussion

In this study, the water droplet transport and dynamics in the novel flow channel are numerically investigated. To better understand the effect of the needle on water transport and dynamics, the water droplet behavior in a conventional channel without the needle is also calculated under the same conditions as the modified channel in the conventional case. For water transport in the base case, the diameter of the needle, D_{needle}, is 0.1 mm and the length of the needle, L_{needle}, is 0.7 mm. The effects of the diameter and length of the needle are also investigated. All the cases considered in the present study are shown in Table 1. In all the cases, the contact angle for the channel wall surface, MEA surface and needle surface are specified as 50°, 140° and 10°, respectively. The gas inlet velocity at the channel inlet, $v_{x,0}$, is taken as 6 m s^{-1}, equivalent to a Reynolds number of 400, when properties of air at room condition are used. The pressure at the channel outlet, P_{out}, is considered as 1 atm. A water droplet with the diameter, $D_{droplet}$, of 0.6 mm was initially introduced on the MEA surface, 1 mm away from the channel inlet. It should be pointed out that the droplet size changes with the current density and humidity conditions in an operating PEMFC. The initial size of the water droplet chosen above is decided based on our experimental observations [40].

It should be further mentioned that in a practical fuel cell, a variety of the MEA/channel orientations may be encountered, i.e., the MEA may be on top and the channel below, or the channel on top of the MEA, or the MEA surface may be vertical. However, the effect of gravity is most favorable for water droplet detachment from the MEA surface when the MEA is on top and the flow channel below. Thus the orientation of the MEA on top of the channel is selected for the present study. On the other hand, the Bond number ($Bo = (\rho g D^2_{droplet})/\sigma$) which represents the ratio of gravitational effect to the surface tension effect is 4.7×10^{-2} by using the water droplet diameter $D_{droplet}$ as the characteristic length as well as the density and surface tension coefficient of water. The relatively small value of Bo number indicates that the surface tension effect is more influential than the gravitational effect. As a result, the influence of the orientation with respect to the gravity is small on the water droplet dynamics for the flow considered in the present study.

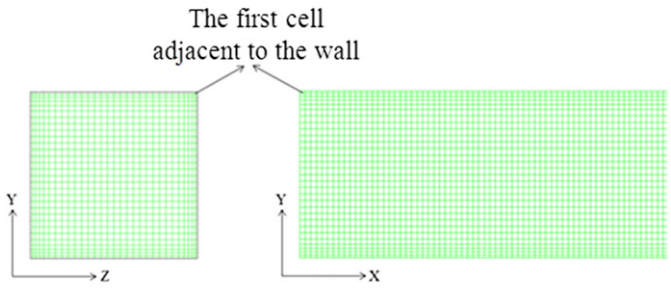

Fig. 3. Computational meshes at the inlet and the channel sidewall.

Table 1
Parameter values considered in the present study.

Cases	Diameter of the needle, D_{needle} (mm)	Length of the needle, L_{needle} (mm)
Base case	0.10	0.70
Conventional case	0	0
Case 1	0.04	0.70
Case 2	0.07	0.70
Case 3	0.15	0.70
Case 4	0.20	0.70
Case 5	0.10	0.40
Case 6	0.10	0.50
Case 7	0.10	0.85
Case 8	0.10	1.00

4.1. Water transport and dynamics in 3D flow channels

A comparison of water transport and dynamics is shown in Figs. 4 and 5 in the two three-dimensional flow channels: the conventional and the modified channel (or the base case) shown in Table 1. In the conventional flow channel, as shown in Figs. 4(a) and 5(a), the water droplet, after being introduced on the MEA surface, is transported only along the MEA surface. This is because the MEA surface is normally hydrophobic, not super-hydrophobic, so that the water droplet still has a considerable contact area on the GDL surface as seen in Figs. 4(a) and 5(a), resulting in a sizable capillary force keeping the water droplet adhering on the GDL surface, Further, the gas velocity in the channel is small near the MEA surface and large away from the surface (near the channel center), resulting in a lift force as well as a rolling moment that makes the droplet rolling on the MEA surface until exiting the channel. These two mechanisms prevent the water droplet from detaching from the MEA surface, as shown in previous studies [29,41].

However, in the modified flow channel with a needle, as shown in Figs. 4(b) and 5(b), the water transport and dynamics behave quite differently; the water droplet is seen to be removed from the MEA surface due to the presence of the low contact angle needle; and once separated from the MEA surface, the droplet is transported downstream without touching the MEA surface again. This is desirable since it renews the MEA surface, clear of liquid water, making it available again for reactant gas transport into the MEA surface – this is the purpose of introducing the needle in the flow channel in the first place.

For the modified channel as shown in Figs. 4(b) and 5(b), at about 6 ms after being introduced into the flow field, the water droplet reaches the needle. Then due to the relatively high capillary effect of the needle which has a contact angle of 10°, the water droplet is transported along the needle towards $-y$ direction, that is, towards the bottom channel surface, away from the MEA surface. At the same time, due to the wall adhesion of the MEA surface and under the large drag force from the air stream, the water droplet

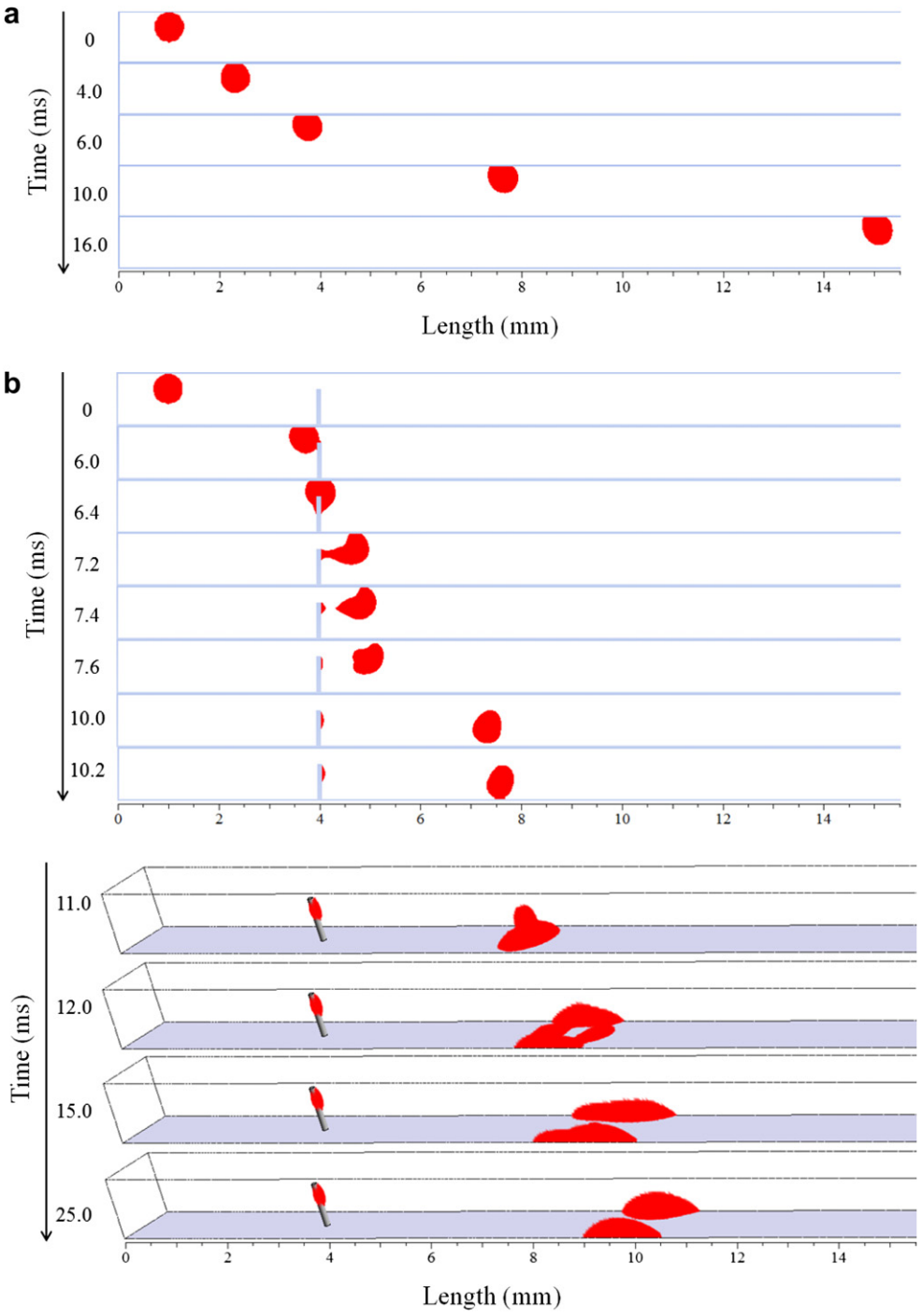

Fig. 4. Numerical results of water transport and dynamics in 3D flow channels: (a) in a conventional flow channel; (b) in the modified flow channel with a needle (base case in Table 1).

moves downstream with its top portion still moving along the MEA surface although the contact area with the MEA surface decreases and the water droplet is being stretched and thinned out at its contact with the needle as the majority of the liquid water is transported downstream. At about 7.4 ms, the droplet breaks off from the needle with a small area of contact with the MEA surface, while only a small part of water is observed still sticking on the needle surface. About 0.1 ms later, the droplet also detaches completely from the MEA surface. From then on, except only a small part of water still sticking on the needle surface, most of the water is transported downstream along with the air stream while at the same time it also moves towards the channel bottom surface. At about 10.2 ms as shown in Fig. 4(b), the water droplet reaches the channel bottom wall. Because the channel bottom wall surface is hydrophilic with a contact angle of 50°, the water droplet upon contact with the bottom channel surface stretches out gradually on the channel surface and spreads to the two bottom corners of the flow channel. Then, due to the strong capillary effect at the corners, the liquid water is separated and contracted towards the two corners of the channel. The separated two parts of water around the

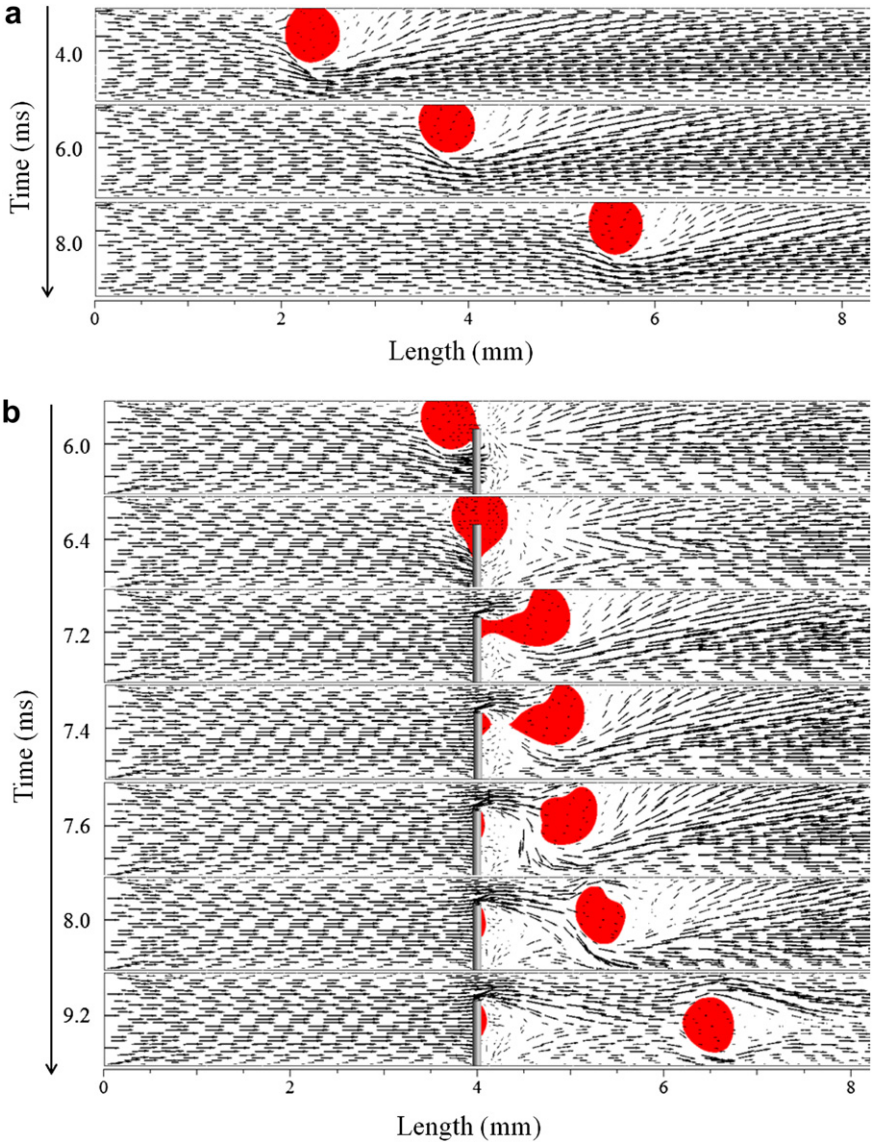

Fig. 5. Flow field (vector plot) in the middle of the 3D flow channels: (a) in the conventional flow channel; (b) in the modified flow channel (base case in Table 1).

two corners are continuously being transported along the two corners towards the outlet direction. It is emphasized again that the water transport behavior in the modified channel is desirable since the MEA surface is free of liquid water, avoiding the flooding and blockage of reactant gas transport into the MEA.

From the above description of the water transport and dynamics in the modified flow channel with a needle, a few parameters of importance are noticed:

- The detaching time T_D: which is the time taken for the water droplet to detach completely from the MEA surface;
- The landing time T_L: which is the time taken for the water droplet to reach the bottom surface of the flow channel;
- The hanging time Δt: which is the time difference between T_D and T_L, or $\Delta t = T_D - T_L$.

In the flow described earlier in the modified channel with a needle, $T_D = 7.5$ ms, $T_L = 10.2$ ms, and thus Δt is 2.7 ms. On the other hand, the same flow in a conventional flow channel without the needle, the water droplet is attached to the MEA surface all the time until it is transported out of the flow channel as shown in Fig. 4(a), that is, T_D approaches infinity. This illustrates the significant effect of the needle on the water transport and removal from the MEA surface. We shall return to these water transport characteristic parameters late.

It should be pointed out that Figs. 4(b) and 5(b) reveal that the hydrophilic needle used in this study facilitates the removal of liquid water droplets from the MEA surface; and at the same time this needle inside the gas channel does not disturb the liquid water flow to the cathode outlet to such a degree that the needle still does not cause "channel plugging". This is because the hydrophilic needle used in this study is very small in diameter so that its surface area (hence its capillary effect) is sufficiently small such that water can easily detach from the needle and be taken away by the reactant gas stream in the channel. Therefore, the size of the needle selected in this study is effective on one hand in removing liquid water from the MEA surface, preventing "water flooding" of MEA; and on the other hand it does not cause "channel plugging", as seen in Figs. 4(b) and 5(b) as well as all the other results obtained in this study some of which are presented later.

It should also be mentioned that the water removal from the MEA surface and the liquid droplet behavior inside the flow channel are largely affected by the gas flow velocity in the channel, and have been investigated for a wide range of gas flow rate typically encountered in the cathode in our earlier studies as shown in [29,41]. For the typical cathode gas flow rates encountered in practical PEMFCs, the general behavior of water removal from the MEA surface through the hydrophilic needle inserted in the flow channel remains the same, as shown in Figs. 4(b) and 5(b) as well as others shown later on in this article, because the needle used in this study is sufficiently small that the gas flow in the cathode is sufficiently strong to take the water droplet away from the needle for typical PEMFC operating conditions, although as the gas flow rate is reduced, the time taken for the water droplet to detach from the MEA surface and then the time taken for the water droplet to reach the bottom surface of the flow channel, that is, the detaching and landing time as defined earlier, will increase.

4.2. Associated pressure drop in 3D flow channels

The pressure drop, ΔP, associated with the flow in the flow channel is the static pressure drop between the inlet and the outlet of the flow channel. Pressure drop for reactant flow through the flow channel is an important parameter in fuel cell operation, since it determines the parasitic losses associated with the reactant gas supply and compression. In some earlier PEM fuel cell power systems operating at elevated pressures, air compression for the cathode air supply consumes as much as 35% of the power output from the stack. For an operating stack or cell, the pressure drop through the flow channel also indicates the extent of the flow maldistribution or the non-uniformity induced in the flow channel due to partial flooding in the channel [38], and/or the change of the available cross section of the flow channel for gas to pass through [25], and hence reflects the blockage of the gas flowing in the channel.

Fig. 6 shows the time evolution of the pressure drop for the 3D flow in the conventional and modified flow channel with a needle (the base case given in Table 1). At the beginning, the pressure drop in both the conventional channel and the modified channel is very high as a result of the sudden presence of the droplet in the channel, and then decreases very quickly to relatively constant values. Within the first several milliseconds, the pressure drop for the modified channel is always greater than for the conventional channel, attributed to the extra pressure drop induced by the presence of the needle in the modified channel. After about 2 ms, the pressure drop for the conventional channel remains almost constant, since the water droplet is transported downstream only along the MEA surface with almost the same shape, as shown in Fig. 4(a) and the flow field around the droplet also remains almost identical at different times as shown in Fig. 5(a). However, the pressure drop for the modified channel increases significantly at about 7 ms, due to the water droplet detaching from the MEA surface and suspending in the flow as shown in Fig. 4(b). This results in the maximum blockage of the water droplet for the flow in the modified channel, hence the spike for the pressure drop. The pressure drop decreases quickly at about 10 ms, when the water droplet reaches the bottom surface of the channel.

As mentioned earlier, when the water droplet reaches the hydrophilic surface of the channel bottom wall at about 12 ms, it spreads quickly into a water film on the surface, decreasing the flow blockage and hence the pressure drop. The water film is further separated and contracted into the two bottom corner areas of the channel until transported out of the channel, as shown in Fig. 4(b), the flow blockage is further reduced, hence the pressure drop reaches an asymptotic constant thereafter. From this time on, it is seen that the pressure drop for the modified channel becomes lower than the corresponding value for the conventional channel. Although there exists an extra pressure drop in the modified channel due to the presence of the needle, it is evident that the pressure drop in the conventional channel, due to the water maintaining droplet shape while in contact with the hydrophobic MEA surface, is substantially larger than the pressure drop in the modified channel where water contracts into thin film form around the corners of the hydrophilic channels.

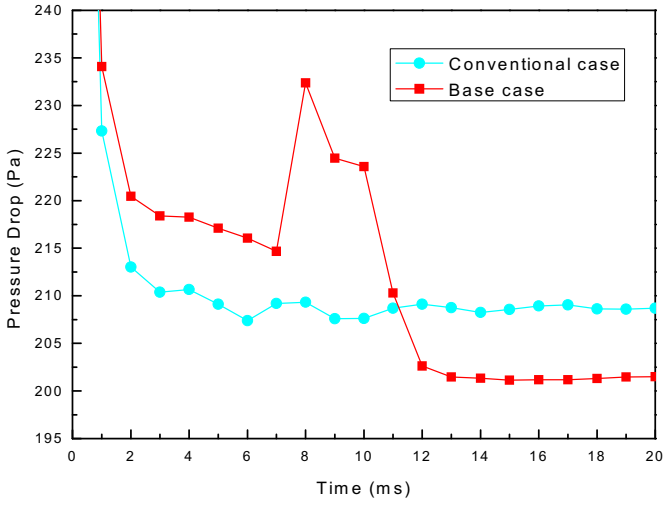

Fig. 6. Pressure drop for the 3D flow in the conventional and the modified flow channels (the modified flow channel is the base case given in Table 1).

For the spike in the pressure drop in the modified channel shown in Fig. 6, it is noticed that the increase occurs around the time T_D when the water droplet detaches from the MEA surface and becomes suspended in the channel flow; while the pressure drop decreases to an asymptotic constant around the time T_L when the water droplet reaches the bottom channel surface. Therefore, the duration of the spike in the pressure drop is approximately equal to the droplet hanging time Δt, or the time duration when the droplet is transported in the channel without touching any of the channel surfaces. This suggests that pressure drop is a useful parameter for the investigation of water transport and dynamics in the flow channel.

4.3. Effect of the needle diameter

The effect of the diameter of the needle has been investigated on the water droplet transport and dynamics in the flow channel. The needle diameter considered includes $D_{needle} = 0$, 0.04, 0.07, 0.1, 0.15 and 0.20 mm, respectively, corresponding to Case 1–4 together with the base case and the conventional case shown in Table 1. Fig. 7 presents the simulated results of water transport and dynamics in the modified flow channel of 1 mm × 1 mm cross section with the needle diameter of 0.04 mm, corresponding to Case 1 shown in Table 1. For this small needle diameter, the transport of the water droplet is hardly affected by the presence of the needle; and the water droplet still travels through the channel with its top surface in contact with the MEA surface, similar to the flow situation in the conventional channel without the presence of a needle.

On the other hand, shown in Fig.8 is the simulated result for the water droplet transport and dynamics in the modified flow channel with the largest needle diameter investigated ($D_{needle} = 0.2$ mm). It is seen that the water droplet is removed from the MEA surface,

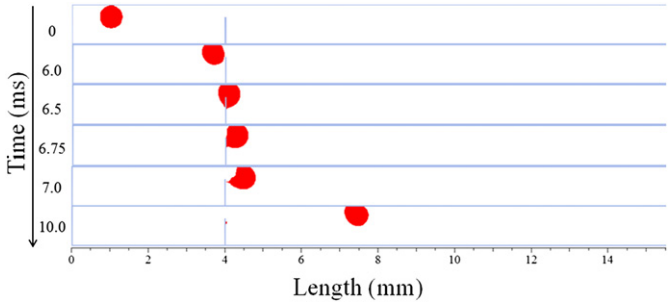

Fig. 7. Numerical results of water transport and dynamics in the modified flow channel for Case 1 given in Table 1.

faster than in the base case where the needle diameter is 0.1 mm, with the detaching time T_D of 7.2 ms and landing time T_L of 8.25 ms. It is noticed that for this case of large needle diameter, the water droplet detaches from the MEA surface before breaking off from the needle, as shown in Fig. 8 at the time of 7.25 ms; in contrast to the base case where the droplet detaches from the needle first, as shown in Figs. 4(b) and 5(b). It is clear that the larger needle diameter gives rise to a stronger capillary effect that holds water longer than the hydrophobic MEA surface, despite the strong air stream in the channel. It is further observed that the strong capillary effect of the large needle diameter also reduces the time for the water droplet to reach the bottom channel surface, the so-called landing time T_L.

The effect of the needle diameter on the water transport characteristic parameters for all the cases studied is summarized in Table 2. It is seen that the needle should be sufficiently large in diameter in order to remove the water droplet from the MEA surface. As the needle diameter is increased, the water droplet becomes easier to detach from the MEA surface and faster to reach the channel bottom surface, i.e., with a smaller value for T_D and T_L. It is noticed that the detachment time T_D is reduced only slightly with an increase in the needle diameter, because the location of droplet detaching from the MEA surface is always near the needle; whereas the landing time T_L is decreased considerably due to the decelerating effect of the needle on the water droplet. As a result, the time between the droplet detaching from the MEA surface to it reaching the bottom channel surface, Δt, is also reduced substantially, like T_L, as the needle diameter is increased.

The effect of the needle diameter on the pressure drop in the flow channel is shown in Fig. 9. It is seen that the pressure drop for Case 1 has a trend of variation similar to the conventional case, and both have no significant spike in the pressure drop, a phenomenon associated with the droplet moving from the MEA surface to the

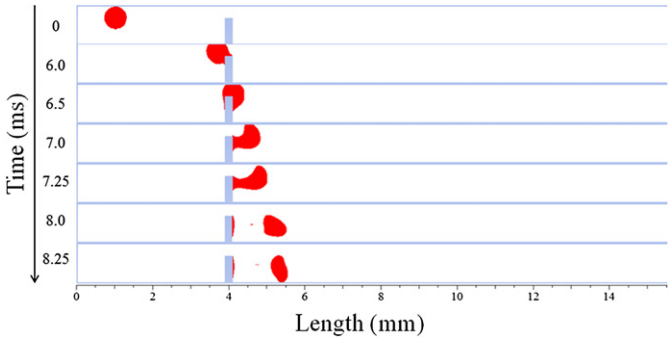

Fig. 8. Numerical results of water transport and dynamics in the modified flow channel for Case 4 given in Table 1.

Table 2
Simulated results for the effect of the needle diameter on the time for the droplet detachment from the MEA surface T_D, the time for the droplet to reach the channel bottom surface, T_L, and the time difference between the two, Δt.

Cases	D_{needle} (mm)	L_{needle} (mm)	T_D (ms)	T_L (ms)	Δt (ms)
Conventional case	0	0	–	–	–
Case 1	0.04	0.70	–	–	–
Case 2	0.07	0.70	7.60	11.25	3.65
Base case	0.10	0.70	7.50	10.20	2.70
Case 3	0.15	0.70	7.40	9.35	1.95
Case 4	0.20	0.70	7.20	8.25	1.05

bottom channel surface, except the small variation associated with the transient droplet dynamics. However, the magnitude of the pressure drop for Case 1 is larger than the corresponding value for the conventional case due to the extra pressure drop caused by the needle. For the needle diameter of 0.07 mm (Case 2) and larger, the pressure drop has a similar trend of variation; and as the needle diameter is increased, the pressure drop is also increased for time $t < T_D$ and $t > T_L$. It is also seen that for time $t < T_D$ the pressure drop increases monotonically with the needle diameter; whereas for time $t > T_L$ the pressure drop for Case 2, where the droplet detaching from the MEA surface and reaching the bottom channel surface occurs, is considerably less than the pressure drop for the conventional case and Case 1 where the droplet is always attached to the MEA surface while being transported through the channel; but for the cases studied where droplet detachment from the MEA surface occurs, the pressure drop is increased with the needle diameter. For the time between the detachment and landing time T_D and T_L, the peak value of the pressure drop is increased while the width of the spike in the pressure drop is reduced as the needle diameter is increased.

As a comparison, the pressure drop for a single-phase air flow is shown in Fig. 10 under the conditions identical to those of Fig. 9 except without the presence of the water droplet. As a result, the increase in the pressure drop shown in this figure is totally caused by the presence of the needle, when compared to the conventional flow channel, equivalent to the needle diameter equal to zero shown in the figure. It is seen that the pressure drop is increased almost linearly with the needle diameter. Therefore, the size of the needle should be optimized, balancing the need for water detachment from the MEA surface and the minimal increase in the

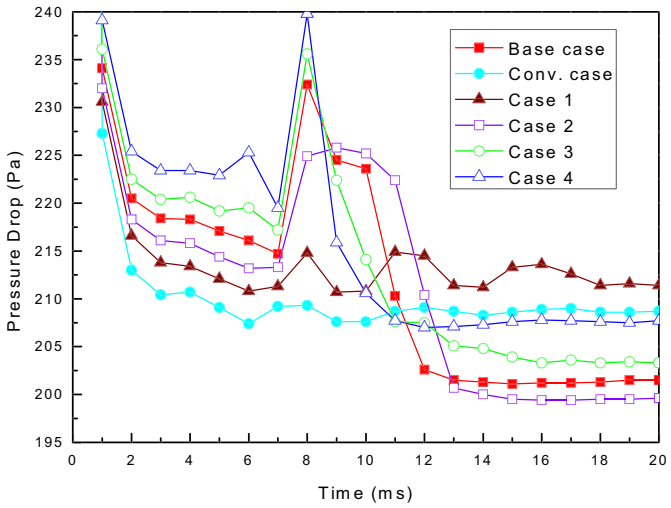

Fig. 9. Effect of the needle diameter on the pressure drop for the 3D flow in the flow channels for the cases given in Table 2 (Conv. case stands for the conventional case).

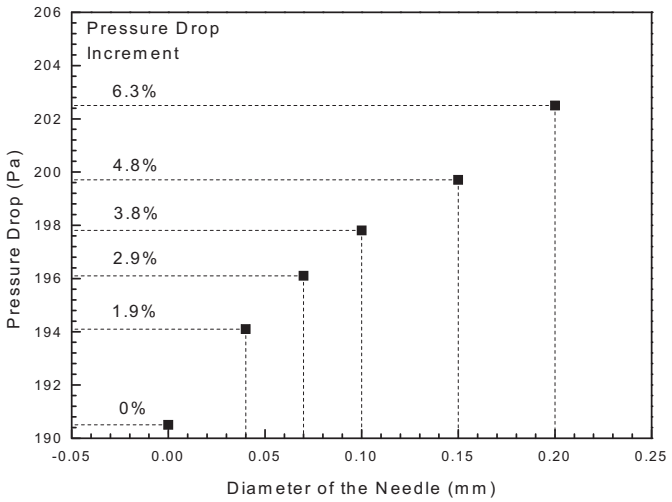

Fig. 10. Effect of the needle diameter on the pressure drop for the single-phase air flow in the 3D flow channels caused by the presence of the needle for the cases given in Table 2.

pressure drop. For the conditions investigated in this study, a needle diameter should be in the range of 0.07–0.10 mm. If a few needles are considered to locate strategically in the flow channel to help water removal process, the resulting pressure drop in the order of a few hundreds of Pa is still much less than the corresponding pressure drop for a serpentine flow channel layout, which could be as high as a few hundreds of kPa [39].

4.4. Effect of the needle length

The effect of the length of the needle is investigated. The length considered includes 0 (conventional case), 0.4, 0.5, 0.7 (base case), 0.85 and 1 mm, respectively, corresponding to the conventional and base cases as well as Case 5–8 shown in Table 1. Fig. 11 shows the results for the water droplet transport and dynamics in the flow channel with the needle length of 0.5 mm (Case 6 in Table 1). It is seen that the water droplet is removed from the MEA surface, but slower than the base case, with the detachment time T_D of about 7.6 ms and the landing time T_L of about 11.0 ms. In this case, the water droplet is barely in contact with the needle top surface and the contact area is much smaller than the base case. For Case 5 where the needle length of 0.4 mm is too short, the gap between

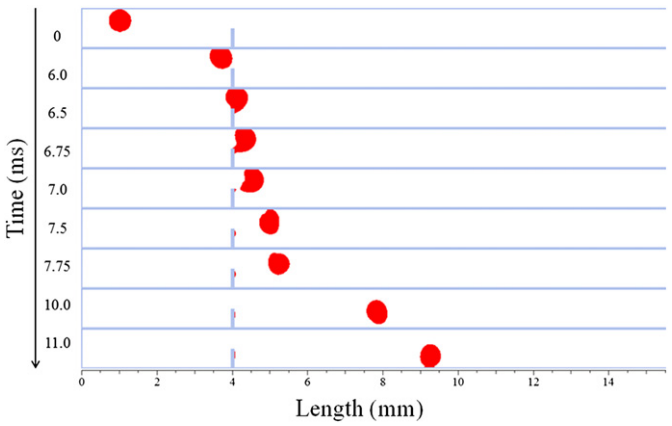

Fig. 11. Numerical results of water transport and dynamics in the modified flow channel for Case 6 given in Table 1.

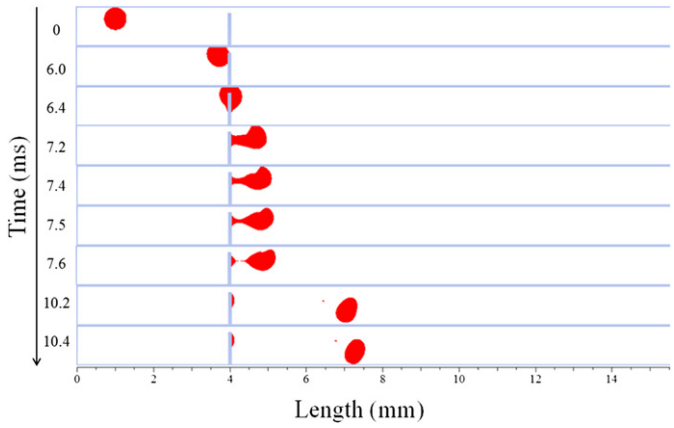

Fig. 12. Numerical results of water transport and dynamics in the modified flow channel for Case 7 given in Table 1.

the needle and the MEA surface is larger than the droplet size so that the droplet cannot contact the needle as it is transported downstream along the MEA surface. As such the droplet transport and dynamics is hardly influenced by the presence of the needle.

The results for the needle length of 0.85 (Case 7) is shown in Fig. 12. It is seen that the water droplet is removed from the MEA surface faster than the base case, with the detachment time T_D of 7.45 ms, due to a greater contact area produced by the longer needle. Hence, water is detached from the MEA surface first, opposite to the base case. However, the landing time T_L is 10.4 ms, longer than the base case. This is because the longer needle having a larger contact area tends to hold the water longer before its break-off occurs; further the longer needle also weakens the air flow above the needle (or in the gap between the needle top and the MEA surface), and consequently weakening the downward air flow behind the needle, reducing the downward force on the water droplet when it is suspending in the air flow, thus delaying droplet reaching the channel bottom surface. This effect of the air flow field is clearly illustrated in the flow field shown in Fig. 13, and when compared with the flow field for the base case shown in Fig. 5(b).

When the needle length is increased to 1 mm (Case 8), so that the needle is now in contact with the MEA surface, as shown in Fig. 14, the water droplet is seen to first become detached from the MEA surface at about 7.4 ms, while it is still attached to the needle. And after detaching from the needle sometimes later, the droplet becomes re-attached to the MEA surface at about 8.0 ms; and

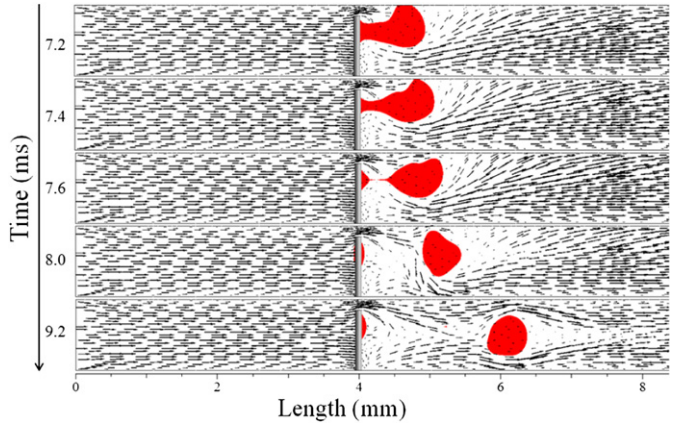

Fig. 13. Flow field (vector plot) in the middle of the flow channel for Case 7 given in Table 1.

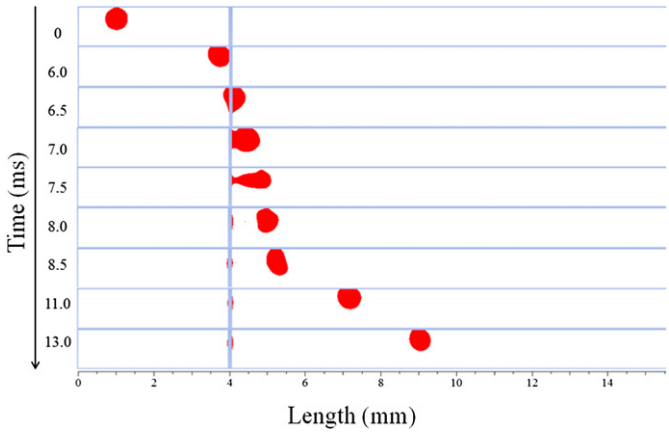

Fig. 14. Numerical results of water transport and dynamics in the modified flow channel for Case 8 given in Table 1.

thereafter the water droplet is transported downstream still in contact with the MEA surface until it is swept out of the channel exit. The corresponding flow field for this case, as shown in Fig. 15, indicates that when the water droplet is about to break off from the needle at about 7.75 ms, the air flow below it is very strong, and thus pushes the droplet upward back to the MEA surface. Or to put it in more detail, the droplet experiences a lift as well as a drag force from the gas flow in the channel, as shown in [29,40], in addition to the capillary force through the touching of the solid surfaces (the needle and the MEA); and the lift force pushes the droplet moving upward against the gravity, resulting into the reattachment of the droplet to the MEA surface.

The effect of the needle length on the water transport characteristic parameters is shown in Table 3 for all the cases investigated in this study. It is seen that the needle should be sufficiently long, at least it should touch the water droplet in order for the water droplet to be removed from the MEA surface. As the length of the needle is increased, the water droplet becomes easier to be removed from the MEA surface by the air stream , and the landing time T_L is reduced correspondingly. However, if the needle length is too long, resulting in excessive contact with the water droplet, the hydrophilic needle tends to hold on the water for a longer period of time during which the water is stretched and deformed, and a strong air flow below the droplet tends to push the water back to re-attach on the MEA surface; hence the landing time T_L is

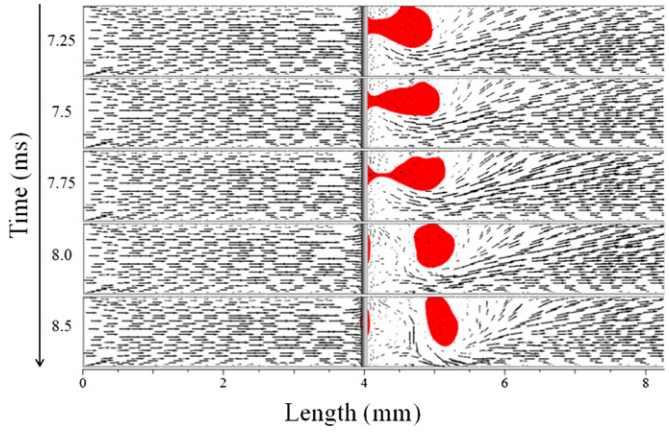

Fig. 15. Flow field (vector plot) in the middle of the flow channel for Case 8 given in Table 1.

Table 3
Simulated results for the effect of needle length on the time for the droplet detachment from the MEA surface T_D, the time for the droplet to reach the channel bottom surface, T_L, and the time difference between the two, Δt.

Cases	D_{needle} (mm)	L_{needle} (mm)	T_D (ms)	T_L (ms)	Δt (ms)
Conventional case	0	0	–	–	–
Case 5	0.10	0.40	–	–	–
Case 6	0.10	0.50	7.60	11.00	3.40
Base case	0.10	0.70	7.50	10.20	2.70
Case 7	0.10	0.85	7.45	10.40	2.95
Case 8	0.10	1.00	7.40	–	–

increased with the needle length, in particular when the needle length is equal to the channel height, the water droplet cannot be removed from the MEA surface any more, or the needle loses its effectiveness on water removal from the MEA surface. Similar to the cases shown in Table 2 for the effect of the needle diameter, the detachment time T_D does not change appreciably with the needle length for the same reason that the location of the water droplet detaching from the MEA surface is always near the needle.

The effect of the needle length on the pressure drop is shown in Fig. 16. It is seen that the characteristics of the effect is very similar to that of the needle diameter shown earlier in Fig. 9. The pressure drop, for the cases (Case 5 and conventional case) where there is no droplet detachment from the MEA surface and for the cases involving droplet detachment from the MEA surface and arrival at the bottom channel surface, behaves almost the same as the corresponding cases shown in Fig. 9. The only difference is for Case 8 where the droplet detaches from the MEA surface first, and then reattaches to the MEA surface later. As a result, the pressure drop has two peaks, the first corresponding to the droplet detachment from the MEA surface, and the second corresponding to the droplet reattachment.

Also as a comparison, Fig. 17 shows the pressure drop in the same flow channels under the identical conditions, except the flow is a single-phase air flow only without the presence of water droplet. As a result, the increase in the pressure drop is completely due to the increase in the needle length. It is seen that the pressure drop increases with the length of the needle, but not in a linear relation. Therefore, the length of the needle should be optimized, balancing the need for water removal from the MEA surface and the minimal increase in the pressure drop. For the conditions investigated in this study, a needle length of 0.7 mm seems to be optimal.

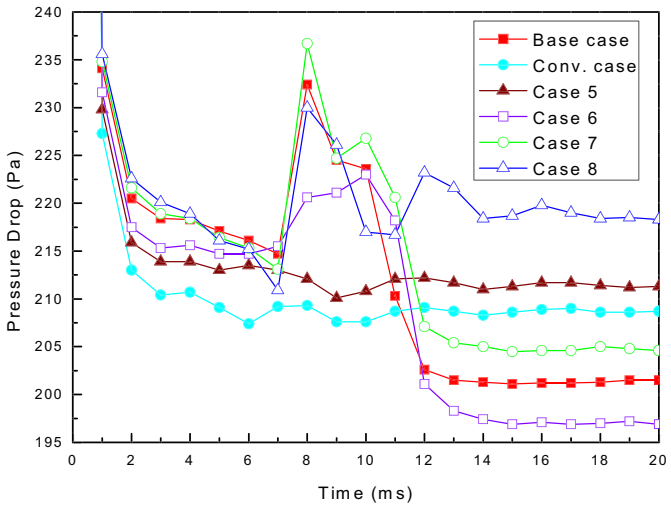

Fig. 16. Effect of the needle length on the 3D pressure drop for the flow in the flow channels for the cases given in Table 3 (Conv. case stands for the conventional case).

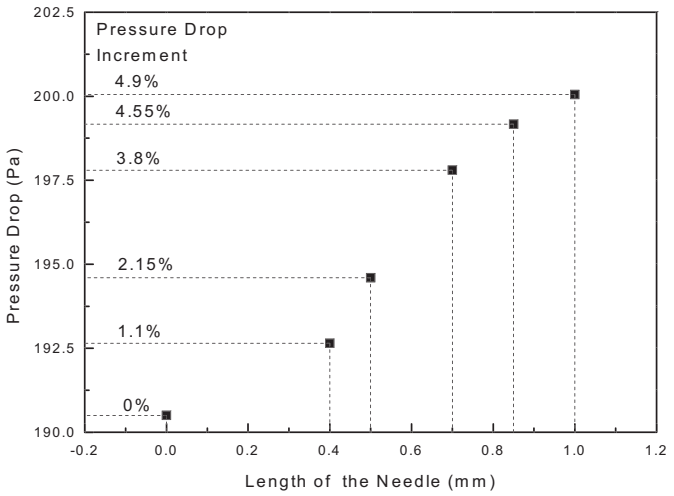

Fig. 17. Effect of the needle length on the pressure drop for the single-phase air flow in the 3D flow channels caused by the presence of the needle for the cases given in Table 3.

Table 4
The effect of multiple needles on the pressure drop in the flow channel.

Number of needles	Pressure drop (Pa)	Increase in the pressure drop (%)
0	190	0
1	198	3.8
2	205	7.7
3	213	11.7
4	220	15.6

Finally, it must be recognized that droplets can emerge randomly in space and time on the MEA surface, and it is indeed fortuitous that the droplet appeared just before the needle as the case considered in this study. Therefore, for practical application multiple needles would have to be used along the length of the channel. Table 4 shows the pressure drop across the flow channel when multiple needles are implemented in the channel. The needles used are the base case defined in Table 1. It is seen that the pressure drop in the channel is increased almost linearly with the number of the needles used, and for three needles the pressure drop is increased by less than 12%, which would still be much less than the corresponding pressure drop if serpentine flow channel is used. It might be visualized that three needles are evenly distributed along the flow channel, at ¼, ½ and ¾ of the channel length. Since water droplet tends to transport along the MEA surface before reaching the needle as shown in Fig. 4(a), the spaced needles would provide an effective means of water removal from the MEA surface.

5. Conclusions

In this study, water droplet transport and dynamics in three-dimensional modified gas flow channels of the proton exchange membrane fuel cell (PEMFC) have been investigated numerically by using the volume-of-fluid method. The conventional flow channel is modified by inserting a small hydrophilic needle in the channel. It is found that optimal diameter and length of the needle exist that balance the need for water removal from the MEA surface and the lower values of the pressure drop for the flow in the channel. For the conditions investigated in this study, the optimal needle has a diameter of 0.1 mm and a length of 0.7 mm. The resulting pressure drop is in the order of a fraction of kPa for a single needle, and could be considered a viable option for water removal in the parallel flow channels of PEMFCs when compared with a serpentine flow channel which could have a pressure drop as high as a few hundreds of kPa, or an excessive parasitic load.

Acknowledgements

This work was financially supported by the National Basic Research Program from the Ministry of Science and Technology of China (973 Program, Grant No. 2010CB234610 and 2012CB215506) and the Natural Science Foundation of Tianjin, China (11JCZDJC23500).

References

[1] P. Quan, M.C. Lai, Journal of Power Sources 164 (2007) 222–237.
[2] K. Jiao, X. Li, Progress in Energy and Combustion Science 181 (2011) 221–291.
[3] T.E. Springer, T.A. Zawodzinski, S. Gottesfeld, Journal of Electrochemical Society 138 (1991) 2334–2342.
[4] T.V. Nguyen, R.E. White, Journal of Electrochemical Society 140 (1993) 2178–2186.
[5] A.Z. Weber, J. Newman, Journal of Electrochemical Society 151 (2004) A311–A325.
[6] M.M. Mench, Q.L. Dong, C.Y. Wang, Journal of Power Sources 124 (2003) 1–9.
[7] R. Satija, D.L. Jacobson, M. Arif, S.A. Werner, Journal of Power Sources 129 (2004) 238–245.
[8] Chuanga PA, Turhana A, Hellera AK, Brenizera JS, Traboldb TA, Mench MM. Third International Conference on Fuel Cell Science, Engineering and Technology. Proceedings Of the FUELCELL; May, 2005, pp. 23–25.
[9] N. Pekula, K. Heller, P.A. Chuang, A. Turhan, M.M. Mench, J.S. Brenizer, K. Unlu, N. Instrum, Nuclear Instruments and Methods in Physics Research A 542 (2005) 134–141.
[10] S. Tsushima, K. Teranishi, S. Hirai, Electrochemical and Solid-State Letters 7 (2004) A269–A272.
[11] K. Jiao, B. Zhou, Journal of Power Sources 169 (2007) 296–314.
[12] K. Jiao, B. Zhou, Journal of Power Sources 175 (2008) 106–119.
[13] K. Jiao, B. Zhou, Journal of Fuel Cell Science and Technology 5 (2008) 041011-1–041011-10.
[14] J. Park, K. Jiao, X. Li, Applied Energy 87 (2010) 2180–2186.
[15] J. Park, M. Matsubara, X. Li, Journal of Power Sources 173 (2007) 404–414.
[16] L. Hao, P. Cheng, Journal of Power Sources 186 (2009) 104–114.
[17] P.K. Sinha, P.P. Mukherjee, C.Y. Wang, Journal of Materials Chemistry 17 (2007) 3089–3103.
[18] D.M. Bernardi, M.W. Verbrugge, AIChE Journal 37 (1991) 1151–1163.
[19] D.M. Bernardi, M.W. Verbrugge, Journal of Electrochemical Society 139 (1992) 2477–2491.
[20] F.Y. Zhang, X.G. Yang, C.Y. Wang, Journal of Electrochemical Society 153 (2006) A225–A232.
[21] I.S. Hussaini, C.Y. Wang, Journal of Power Sources 187 (2009) 444–451.
[22] K. Jiao, J. Park, X. Li, Applied Energy 87 (2010) 2770–2777.
[23] J.L. Zhang, H. Li, Z. Shi, J.J. Zhang, International Journal of Green Energy 7 (2010) 461–474.
[24] P. Quan, B. Zhou, A. Sobiesiak, Z. Liu, Journal of Power Sources 152 (2005) 131–145.
[25] K. Jiao, B. Zhou, P. Quan, Journal of Power Sources 154 (2006) 124–137.
[26] K. Jiao, B. Zhou, P. Quan, Journal of Power Sources 157 (2006) 226–243.
[27] Z. Zhan, J. Xiao, M. Pan, R. Yuan, Journal of Power Sources 160 (2006) 1–9.
[28] Y.H. Cai, J. Hu, H.P. Ma, B.L. Yi, H.M. Zhang, Journal of Power Sources 161 (2006) 843–848.
[29] B. Mondal, K. Jiao, X. Li, International Journal of Energy Research 35 (2011) 1200–1212.
[30] X. Zhu, Q. Liao, P.C. Sun, N. Djilali, Journal of Power Sources 195 (2010) 801–812.
[31] J.J. Baschuk, X. Li, Applied Energy 86 (2009) 181–193.
[32] C.T. Wang, Y.C. Hu, P.L. Zheng, Applied Energy 87 (2010) 1366–1375.
[33] S.W. Perng, H.W. Wu, T.C. Jue, K.C. Cheng, Applied Energy 86 (2009) 1541–1554.
[34] H.W. Wu, H.W. Ku, Applied Energy 88 (2011) 4879–4890.
[35] S. Patel, A.S. Bansode, T. Sundararajan, S.K. Das, International Journal of Green Energy 5 (2008) 35–54.
[36] X. Li, I. Sabir, International Journal of Hydrogen Energy 30 (2005) 359–371.
[37] ANSYS FLUENT 12.1 User's Guide, ANSYS Inc., 2009.
[38] X. Zhu, P.C. Sun, N. Djilali, Journal of Power Sources 181 (2008) 101–115.
[39] X. Li, I. Sabir, J. Park, Journal of Power Sources 163 (2007) 933–942.
[40] S.A. Shakhshir, Y. Wang, I. Alaefour, X. Li, ECS Transactions 42 (2012).
[41] Mondal B., Jiao K, Li X. Three-dimensional simulation of water droplet movement in PEM fuel cell flow channels with hydrophobic surfaces. International Journal of Energy Research. Accepted.